*Acta Oceanol. Sin.*, 2018, Vol. 37, No. 3, P. 21–30
DOI: 10.1007/s13131-018-1197-1
http://www.hyxb.org.cn
E-mail: hyxbe@263.net

# Numerical simulations of rip currents off arc-shaped coastlines

WANG Hong[1, 3], ZHU Shouxian[2*], LI Xunqiang[1], ZHANG Wenjing[1], NIE Yu[1]

[1] Institute of Meteorology and Oceanography, National University of Defense Technology, Nanjing 211101, China

[2] College of Oceanography, Hohai University, Nanjing 210098, China

[3] 91937 Troops, Zhoushan 316000, China

Received 20 April 2017; accepted 31 May 2017



**Abstract**

The rip currents induced by waves off arc-shaped coastlines are seriously harmful to humans, but understanding of their characteristics is lacking. In this study, the FUNWAVE model was used to calculate the wave-induced currents in the Haller experiment and the ideal arc-shaped coast similar to Sanya Dadonghai, Hainan Province, China. The results showed that the FUNWAVE model has considerable ability to simulate the rip currents, and it was used to further simulate rip currents off arc-shaped coastlines to investigate their characteristics. The rip currents were found to be stronger as the curvature of arc-shaped coastline increased. Coastal beach slope exerts a significant influence on rip currents; in particular, an overly steep or overly mild slope is not conducive to creating rip currents. Furthermore, the rip currents were found to become weaker as the size of arc-shaped coast decreased. When the height and period of waves increase, the strength of rip currents also increases, and, in some cases, wave heights of 0.4 m may produce dangerous rip currents.

**Key words:** rip current, arc-shaped coastline, FUNWAVE model, numerical simulation

**Citation:** Wang Hong, Zhu Shouxian, Li Xunqiang, Zhang Wenjing, Nie Yu. 2018. Numerical simulations of rip currents off arc-shaped coastlines. Acta Oceanologica Sinica, 37(3): 21–30, doi: 10.1007/s13131-018-1197-1

## 1 Introduction

In the process of wave propagation from deep to shallow water, affected by changes of topography, the waves roll back and break, sometimes producing relatively strong offshore flows called rip currents (Bowen, 1969). Previous studies have obtained crude estimates of rip current velocities, such as 0.3–1 m/s (MacMahan et al., 2006), 2 m/s and sometimes 3 m/s (Short, 2007). Rip currents, which are rapid offshore-directed jets of water that originate in the surf zone and broaden outside the breaking regions with high speed, not only exert an important effect on the transport of sediments and pollutants (Jin et al., 2006; Brown et al., 2009), but may also take swimmers of all ability levels into deeper water within minutes, causing casualties (Choi et al., 2013). Australia had about 25 000 beach drowning incidents each year, of which 89% were related to rip currents (Short, 2007). Eighty percent of the beach drowning rescues in the United States were related to rip currents, and more than 100 people died each year from beach drowning (Lascody, 1998).

An arc-shaped coastline is a common type of coastline, where rip currents occur frequently, leading to drownings. Dalrymple et al. (2011) believed that the occurrence of rip currents off an arc-shaped coastline is due to the wave-crest line deformation that forms strong and weak wave energy zones that causes the rip currents. There are many arc-shaped coasts in China that are prone to rip currents. Though statistics are incomplete, Dadonghai, which is a famous bathing beach in Sanya, Hainan Province, has been the site of hundreds of drownings owing to rip currents; 38 people died at Dadonghai between 2004 and 2013 (Li and Zhu, 2015). However, because of the lack of field observation, the characteristics of rip currents on such arc-shaped beaches are still not well understood.

Many scholars have analyzed the characteristics of rip currents by conducting physical experiments in harbor pools (Dean and Oh, 1994; Haller et al., 1997, 2002; Haas and Svendsen, 2002; Drønen et al., 2002; Kennedy and Thomas, 2004; Castelle et al., 2010). The initial method of rip current field observation was a combination of visual observation and deployment of electronic flow-rate sensors, but in recent years GPS floats and aerial photography have been used more frequently (Wang and Zou, 2014), along with satellite remote sensing (Li and Zhu, 2015) and the use of dye tracers (Huntley et al., 1988). However, because of the instability and complexly spatial structure of rip currents (Giger et al., 1991), it is difficult to catalog accurate descriptions of their characteristics by field observation. It is also difficult to accurately distinguish between rip currents and tidal currents by field observation because the rip currents change quickly owing to the variations in tide and wave actions. Therefore, some scholars have analyzed the characteristics of rip currents using numerical simulations (Chen et al., 1999; Fang et al., 2011; Castelle and Coco, 2012; Bae et al., 2013; Shin et al., 2014; Ha et al., 2014). Chen et al. (1999) tested the effectiveness of FUNWAVE model in rip current simulations by using wave laboratory experimental data, and then studying the rip current mechanisms based on numerical simulations. Bae et al. (2013), Shin et al. (2014), and Ha et al. (2014) all used FUNWAVE model to simulate the rip currents at Haeundae Beach, Busan, South Korea, tested the simulations by CCTV remotely sensed imagery, and analyzed the characteristics and dynamic mechanisms of rip currents on the beach

Foundation item: The National Natural Science Foundation under contract Nos 41206163, 41076048 and 41376012; the Operation Expenses for Universities' Basic Scientific Research of Central Authorities under contract Nos 2011B05714 and 2014B06514.
*Corresponding author, E-mail: zhushouxian@vip.sina.com

based on numerical simulations. Castelle and Coco (2012) studied the rip current patterns on an ideal embayed beach based on the nonlinear hydrodynamic model, tested the simulations using video imaging, and studied the evolution of rip currents using the simulations.

There are two types of models currently used to simulate rip currents. One is the wave-resolved model, which describes the wave-particle motions that allow the wave heights to be determined. The wave average of the motions of wave particles results in wave-induced flows and rip currents. The wave-resolved model mainly uses the Boussinesq or Navier-Stokes equations. Another type of model is the wave-averaged model, which directly describes the wave-averaged motions. It uses the wave-averaged hydrodynamic equations, including the radiation stress and surface rollers from the wave model, to simulate both wave-induced flows and rip currents. It is usually coupled with the wave model. In this paper, the FUNWAVE model based on the Boussinesq equations is used to simulate rip currents, and their characteristics off arc-shaped coastlines are analyzed based on the simulations.

## 2 Test of FUNWAVE model in simulating rip currents

In this study, FUNWAVE, a nonlinear Boussinesq model developed at the University of Delaware (USA), is used to simulate wave-induced currents. It is one of the most advanced models for simulating wave-induced flows, and has been used for the investigation of rip currents in many previous studies (Shi et al., 2012). Owing to the lack of field observation data, data from wave laboratory experiments, remote sensing, and photography were used in testing the numerical simulations of rip currents in previous studies (Chen et al., 1999; Hass et al., 2003; Fang et al., 2011; Castelle and Coco, 2012; Bae et al., 2013; Shin et al., 2014; Ha et al., 2014). We also quantitatively tested the numerical simulations of rip currents using Haller's wave laboratory experiment data, and made qualitative comparisons to the numerical simulations and the photography of rip currents on an ideal arc-shaped coast like Dadonghai Beach. There is no standard definition for defining rip currents. Short (2007) defined a rip current as an offshore flow with a speed above 0.3 m/s, and we also adopt this standard.

Haller et al. (1997) measured wave breaking and rip currents on a barred beach in a laboratory experiment. As shown in Fig. 1, the basin of Haller experiment has a constant water depth of 0.363 m. There are three bars, and the water depths at the shore toe and on the crest of the bar are 0.1 m and 0.048 m, respectively. A normally incident regular wave with period of $T$=1 s and a height of $H$=0.048 m was induced. The wave height and mean water level were observed in the sections of A ($y$=1.1 m), B ($y$=4.6 m) and C ($y$=7.6 m) as shown in Fig. 1a, and the wave-induced flows were observed in the sections of D ($x$=10.0 m), E ($x$=11.25 m), F ($x$=12.3 m) and G ($x$=13.0 m).

In some previous numerical simulations (Fang et al., 2011; Chen et al., 1999), the slope variation from long-shore uniformity in the planar beach was neglected, the slope in Fig. 1b was simplified as 1:30 and only an idealized half of the bathymetry was used to reduce the amount of computation. In this study, we also take half of the experimental area as the computational domain. The topography of the simulation is shown in Fig. 2a, in which the slope is averaged as 1:30. The grid-space and time-step increments are $\Delta x$=0.05 m, $\Delta y$=0.1 m, and $\Delta t$=0.01 s. Waves are generated by the source function technique as detailed by Wei et al.

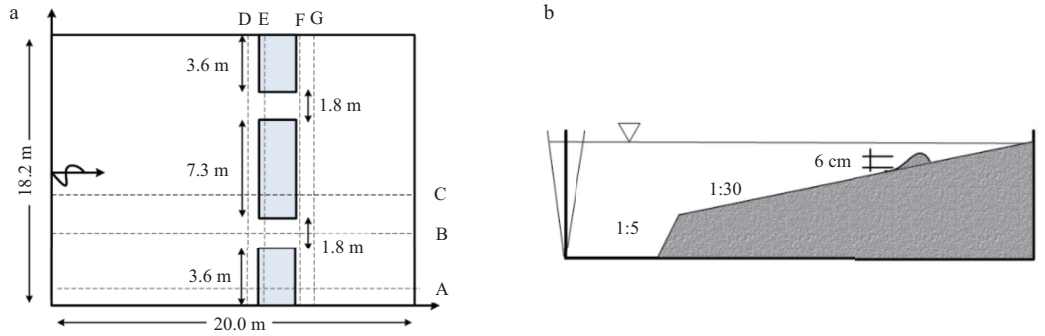


**Fig. 1.** Plan view (a) and cross-section (b) of Haller experiment.

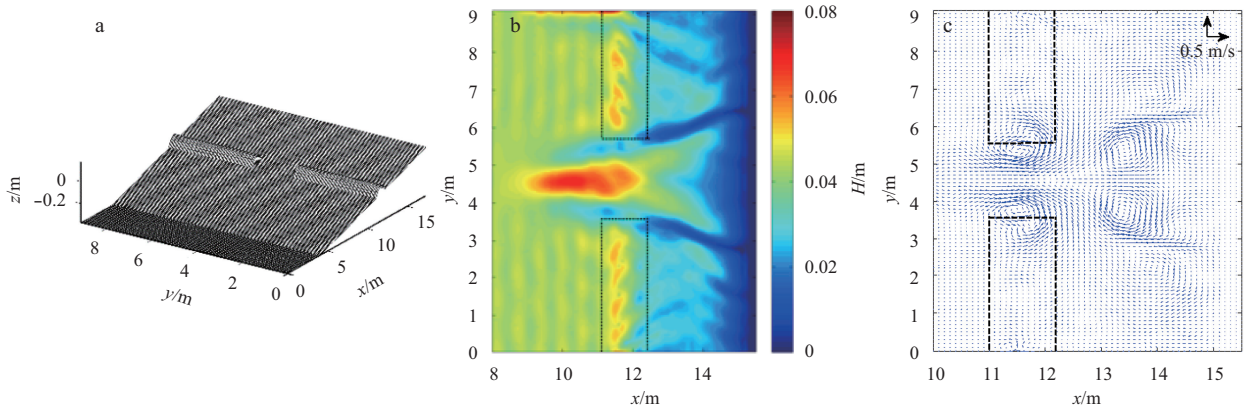


**Fig. 2.** Topography and results of the numerical simulation for Haller experiment. a. Numerical topography, b. wave height ($H$), and c. wave-induced current.

(1999). The wave generation is located internally at $x$=2.5 m, and a damping sponge layer is put behind the source line to absorb outgoing waves reflected by the submerged bar and the sloping beach. The computed datasets from 20 to 200 s are used for statistical analysis. The computed wave height is plotted in Fig. 2b: when the wave climbed over the sand bar to reach shallower water, the wave height increased, broke, and then weakened rapidly. The waves breaks on the submerged bar and near the shoreline on the barred beaches, while at the rip channel, wave breaking mainly occurs near the shoreline. The simulation results of wave-induced flow are given in Fig. 2c. There are two strong offshore currents in the rip channel, and the maximum speed of flow velocity is 0.35 m/s, which is in accord with rip current characteristics.

The computed wave height and mean water level (MWL) along three cross-shore transects are plotted in Fig. 3. The experimental data and the numerical results from Chen et al. (1999) and Fang et al. (2011) are also presented. The long-shore mean current ($U$) and the cross-shore mean current ($V$) are compared to the experimental data and the numerical results from Chen et al. (1999) and Fang et al. (2011) in Figs 4 and 5, respectively. Generally, the simulated results from this study agree well with the numerical results of Chen et al. (1999) and Fang et al. (2011), and are very close to the experimental results of wave height, MWL, and wave-induced flow. The average error of wave height between the numerical results and the observed values in the three sections $y$=1.1 m, 4.6 m and 7.6 m is 0.45 cm, and the average error of mean water level is 0.58 mm. The average error of long-shore mean current at the four sections $x$=10.0 m, 11.25 m, 12.3 m and 13.0 m is 0.038 1 m/s, and the average error of cross-shore mean current is 0.029 7 m/s. The numerical simulation results from Haller experiment show that the FUNWAVE model can qualitatively and quantitatively reproduce waves and wave-induced currents near shore, especially the characteristics of rip currents.

Although there are no on-site measurements of rip currents at Dadonghai Beach, we can examine them using remote-sensing-satellite image and photograph. The CCTV image (Li, 2016) in Fig. 6a shows rip currents at Dadonghai Beach with the zone indicated by the dotted line. Another snapshot in Fig. 6b also presents the rip currents between two surf zones at Dadonghai Beach. According to the real depth, and the real shape and size of the Dadonghai coastline, an ideal arc-shaped coastline is designed as shown in Fig. 7a, with the coastline and water depth in the shape of a parabola. The area for calculation measures 700× 1 000 m$^2$, and the grid spaces are $\Delta x$=1.5 m and $\Delta y$=2.0 m. The wave generation is located internally at $x$=80 m, and a damping sponge layer is also put behind the source line. The normally incident regular wave with $T$=7.0 s and $H$=0.6 m is set. The computed datasets over five periods after the model has run for 1 500 s are used in the statistical analysis. The results of simulated height are given in Fig. 7b and those of wave-induced flow in Fig. 7c. Figure 7d presents the range of rip currents with offshore speed above 0.3 m/s.

The simulated rip currents can be explained mainly by the wave-induced radiation stress. Macmahan et al. (2006) used the following equations to analyze the mechanisms of rip current:

$$\frac{\mathrm{d}S_{xx}}{\mathrm{d}x}=-\rho g(h+\bar{\eta})\frac{\mathrm{d}\bar{\eta}}{\mathrm{d}x}, \tag{1}$$

$$F_y=-\frac{\mathrm{d}S_{yy}}{\mathrm{d}y}-\rho g(h+\bar{\eta})\frac{\mathrm{d}\bar{\eta}}{\mathrm{d}y}, \tag{2}$$

where the $S_{xx}$ and $S_{yy}$ are the radiation stresses, $\bar{\eta}$ is the mean water level and $h$ is the still water depth, $\rho$ is the density of seawater and $g$ is the gravitational acceleration. Considering the cross-shore ($x$) momentum equation, the changes of $S_{xx}$ are balanced by the hydrostatic pressure gradient. Applying linear wave theory in shallow water, $S_{xx}$=3/2$E$, where $E$ is the wave energy and proportional to the square of wave height. The $S_{xx}$ results in wave

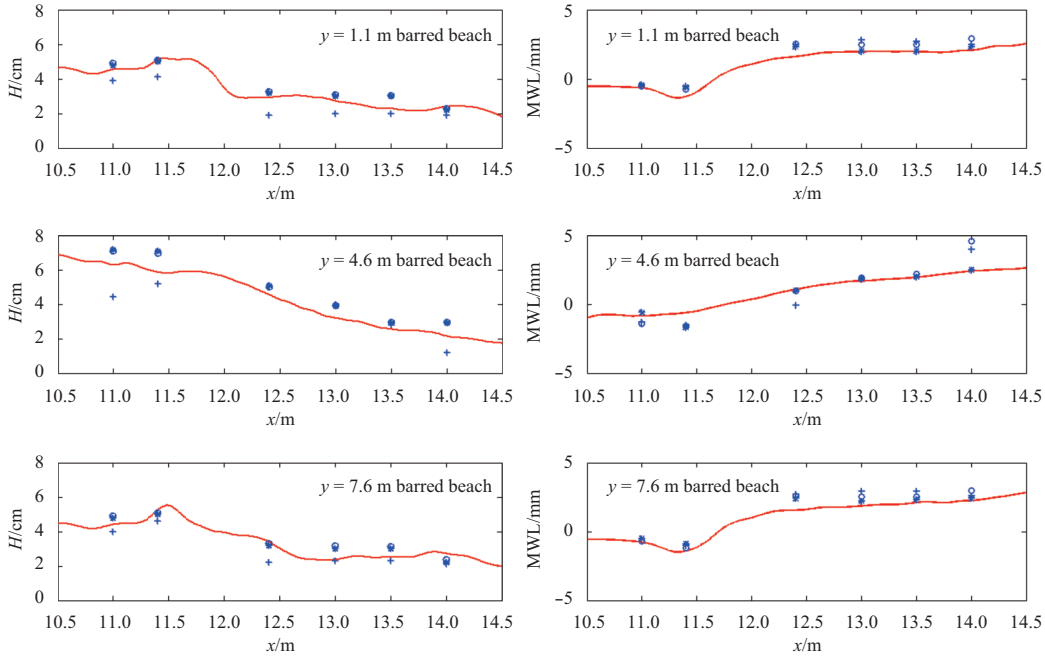


**Fig. 3.** Comparisons of simulated wave height and mean water level from this study (solid line), Chen et al. (1999) (asterisks), Fang et al. (2011) (circles), and measurements (plus signs).

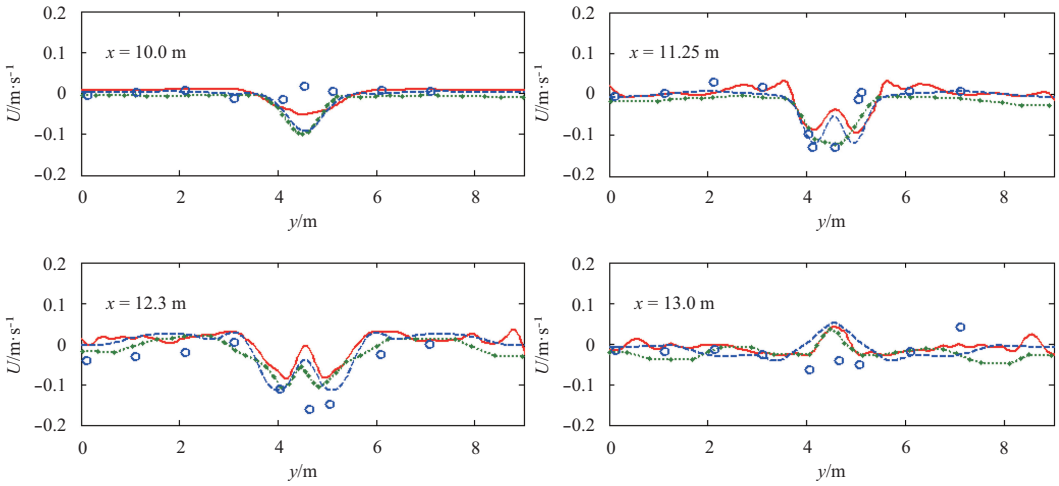


**Fig. 4.** Comparisons of long-shore mean current ($U$) from numerical results of this study (red solid line), Chen et al. (1999) (cyan dashed-dotted line), Fang et al. (2011) (blue dashed line), and measurements (open circles).

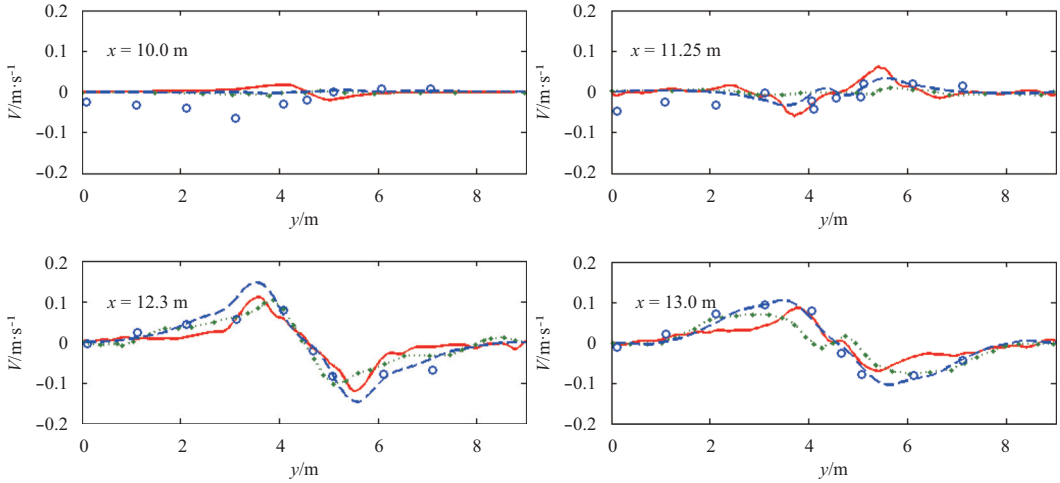


**Fig. 5.** Comparisons of cross-shore mean current ($V$) from numerical results of this study (red solid line), Chen et al. (1999) (cyan dashed-dotted line), Fang et al. (2011) (blue dashed line), and measurements (open circles).

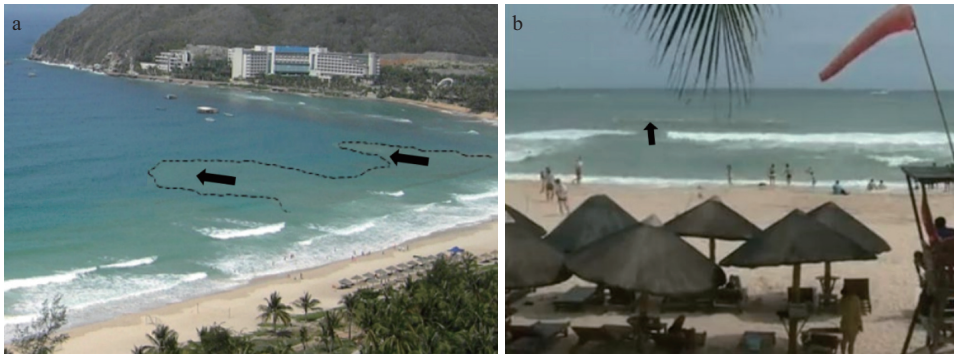


**Fig. 6.** The snapshots of rip currents at Dadonghai Beach. Arrows indicate the positions of rip currents.

set-down outside the surf zone as the wave energy increases due to shoaling, and set-up inside the surf zone as the waves break and the energy decreases. Considering the alongshore ($y$) momentum equation, inside the surf zone, the gradients in the alongshore radiation stress and pressure act together to produce a flow of water from the regions of high waves to the regions of low waves. As shown in Fig. 7a, the water depth at the both sides is shallower than that at the center of the coast, thus the simulated wave height in Fig. 7b generally increases from the center to the sides, and the low waves are near the section $y$=500 m. The alongshore currents in Fig. 7c also flow from the side to the top of the coast, and then turn offshore. The strong rip currents in Fig.

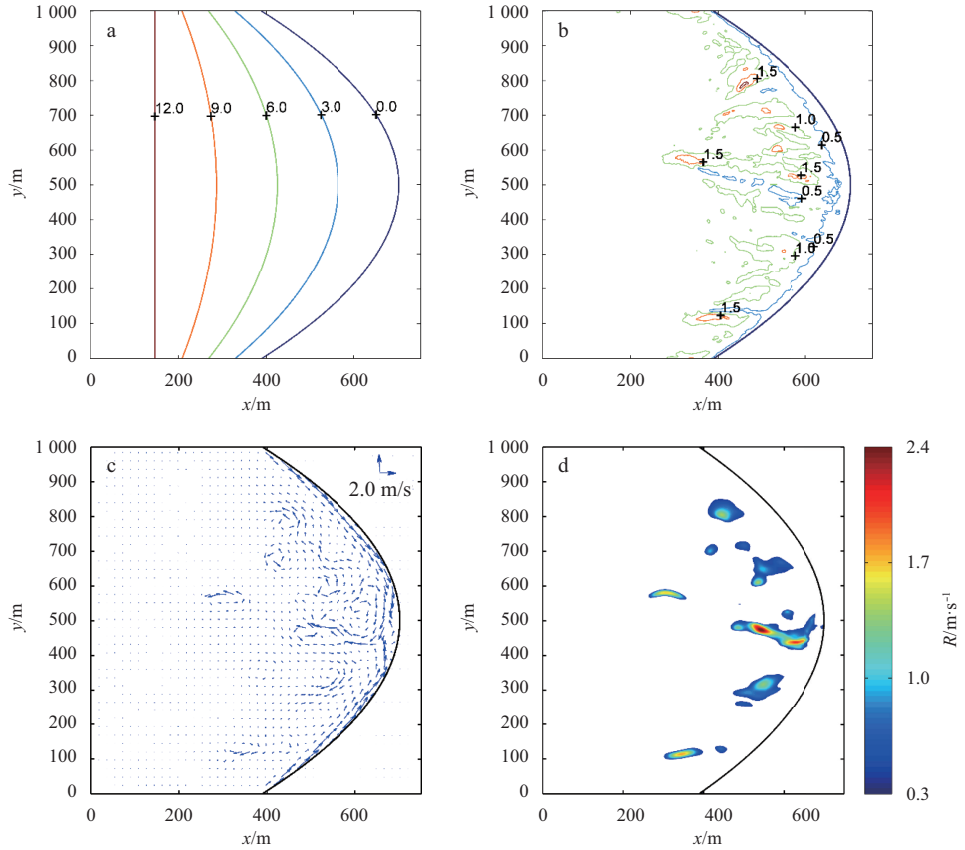


**Fig. 7.** Simulated results of rip currents off an ideal arc-shaped coastline. a. Contours of still water depth (unit: m), b. simulated wave height (unit: m), c. wave-induced flow (unit: m/s), and d. range of rip currents velocity (unit: m/s). *R* denotes rip current velocity.

7d are near the section *y*=500 m, with the maximum speed of 2.46 m/s and the maximum width of 246 m.

## 3 Numerical simulations of the influence of wave height and period on rip currents

Some numerical simulations were carried out by setting the coastal terrain as in Fig. 7a and changing the incident wave height and period, the results of which are shown in Table 1. The first group of simulations retain a wave period of $T$=7.0 s, but use incident wave heights of 0.1, 0.4, 0.5, 0.7 and 1.5 m. The results from the first group of simulations show that the maximum speed, penetration distance and area of rip currents increase as the incident wave height increases. The second group of simulations retain an incident wave height of $H$=0.6 m, but use wave periods of 2.0, 4.0, 7.0, 10.0 and 15.0 s. The maximum speed, penetration distance and area of rip currents increase as wave period increases. However, when the wave period increase from 10 s to 15 s, the area of the rip currents is relatively stable.

In the case of wave period $T$=7.0 s and wave height $H$=0.4 m, a large range of rip currents is still in the simulation results, with a maximum speed of 1.49 m/s. Shin et al. (2014) simulated the rip currents generated by honeycomb-patterned wave trains in a 500×700 m$^2$ region with a simple slope. They set the incident wave height at 0.4 m and the wave period at 8.0 s, and obtained a maximum speed of 1.2 m/s for their simulated rip currents. The results from this study and of that of Shin et al. (2014) show that the significant rip currents may be driven by incident waves of small height in some special cases.

We also made the numerical simulation by the irregular wave, in which the TMA spectra was adopted with the significant wave height of 0.6 m and peak wave period of 7.0 s. The spreading parameter of directional spectrum and the peakedness parameter of frequency spectrum were taken as $\gamma$=6.6 and $\sigma_\theta$=10°, respectively. The simulated maximum speed of rip currents is 1.86 m/s, which is 75% of that in Fig. 7d. So the numerical simulations with regular waves may over-predict the magnitude of rip currents. We will observe the rip currents at Dadonghai Beach later, then make more discussions on the numerical simulations with regular and irregular waves.

## 4 Numerical simulations of the influence of the curvature of an arc-shaped coastline on rip currents

In the actual physical area studied, the curvature of arc-shaped coastline is different, and we ran various numerical simu-

**Table 1.** Statistics for rip currents of various incident wave heights and periods

| | Group 1 ($T$=7.0 s) | | | | | Group 2 ($H$=0.6 m) | | | | |
|---|---|---|---|---|---|---|---|---|---|---|
| | $H$=0.1 m | $H$=0.4 m | $H$=0.5 m | $H$=0.7 m | $H$=1.5 m | $T$=2.0 s | $T$=4.0 s | $T$=7.0 s | $T$=10.0 s | $T$=15.0 s |
| Maximum speed of rip current/m·s$^{-1}$ | 0.36 | 1.49 | 1.99 | 2.70 | 3.68 | 1.32 | 1.67 | 2.46 | 2.51 | 2.63 |
| Penetration distance of rip current/m | 28 | 134 | 187 | 259 | 352 | 119 | 162 | 246 | 241 | 257 |
| Area of rip current/m$^2$ | 192 | 21 225 | 32 625 | 58 041 | 78 300 | 12 906 | 26 802 | 44 739 | 48 444 | 47 370 |

lations of rip currents by changing the arc-shaped coastline's curvature. The common characterization of the curvature $k$ of an arc-shaped coastline (Hsu et al., 1989; Li et al., 2014) is defined as $k$=$L_s$/$L_c$, shown in Fig. 8a, where $L_s$ is the shoreline length and $L_c$ is the embayment width. Five arc-shaped coastlines with different curvatures are shown in Fig. 8b. The coastline is in the shape of a parabola, the shoreline length is 1 000 m, and the water depth of the flat bottom is 12.0 m. However, the embayment widths are $L_c$ =500, 300, 200, 100 and 30 m, which correspond to curvature values of 0.5, 0.3, 0.2, 0.1 and 0.03, respectively. The incident waves are the same, with wave height $H$=0.6 m and period $T$=7.0 s. The computed datasets over five periods after running the model for 1 500 s are selected in order to analyze the wave-induced currents, which are shown in Figs 9a, c, e, g and i. We also give the ranges of rip currents in Figs 9 b, d, f, h and g. The wave-induced currents for these five arc-shaped coastlines all flow similarly along the shoreline to the top, and then turn offshore. However, their intensities become weaker as their curvatures decrease, with absolute maximum speeds of 3.95, 3.09, 2.79, 1.88 and 1.06 m/s, respectively. The rip currents decrease significantly in intensity and range as the curvatures decrease, with maximum speeds of 2.59, 2.46, 1.99, 1.36 and 0.48 m/s and range areas of 49 305, 44 739, 31 011, 19 551 and 5 124 m$^2$, respectively. And the penetration distances of rip current are 322, 246, 183, 128 and 61 m. In these simulations, when the curvature of coastline is 0.03, the rip currents can be neglected.

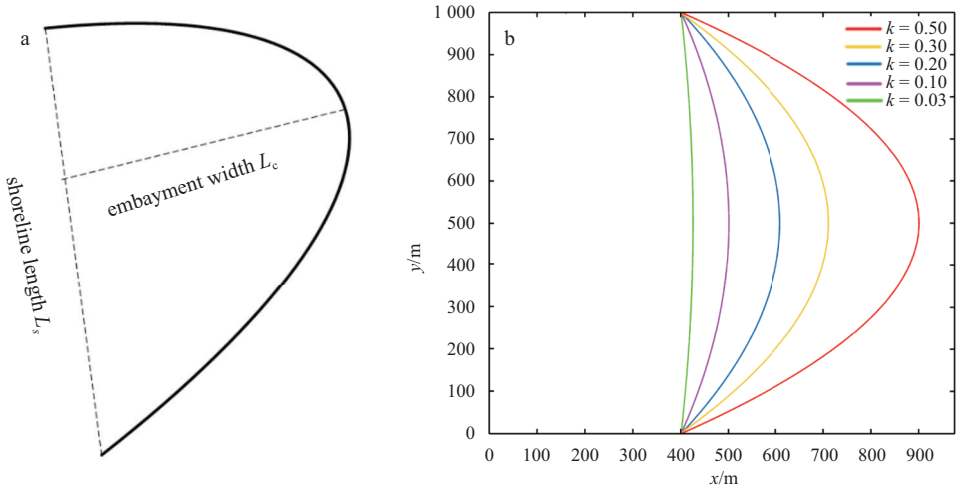


**Fig. 8.** Terrain details of arc-shaped coastline. a. Arc-shaped coastline morphological characteristics, and b. plan view for different curvatures of arc-shaped coastline.

The simulated results of wave height for the coastlines with $k$=0.5 and $k$=0.03 are presented in Figs 10a and b, respectively. Induced by the large curvature of $k$=0.5, the high waves are distributed at the two sides with the maximum height larger than 1.5 m, and the low waves at the center have the height lower than 0.5 m. While off the coastline with $k$=0.03, the high waves at the two sides only have the height about 1.0 m, and there is no obvious low waves at the center. The gradients of wave height from the sides to the center off the little curvature coastline are not so stronger as those off the large curvature coastline, which result in the differences of rip currents in Figs 9b and j.

## 5 Numerical simulations of the influence of coastal slope on rip currents

Numerical simulations were also run by setting three arc-shaped coasts with different slopes. As shown in Fig. 11, these arc-shaped coasts have the same water depth of flat bottom 18 m, but with different slope. Figure 11b shows a cross-section of $y$=500 m, the position marked by a red X is the boundary between water and land, and the slopes of the arc-shaped coasts with the aforementioned water depths are Slope_1=0.015, Slope_2=0.04, and Slope_3=0.063 6, respectively. The numerical simulations have the same incident wave of height 0.6 m and period 7.0 s, and the results over five periods after running the model for 1 500 s are used to analyze the wave-induced and rip currents. Figures 12a, c and e present the distributions for the wave-induced currents, and Figs 12b, d and f present those for the range of rip currents. In the numerical simulation with a coastal slope of 0.015, the absolute maximum speed of wave-induced currents is 1.79 m/s, and the maximum speed, penetration distance and area of rip currents are 1.45 m/s, 242 m and 19 605 m$^2$, respectively. And in the numerical simulation with a coastal slope of 0.04, the absolute maximum speed of wave-induced current is 3.28 m/s, the maximum speed, penetration distance and area of rip currents are 2.21 m/s, 162 m and 31 713 m$^2$. While in the numerical simulation with a coastal slope of 0.063 6, the absolute maximum speed of wave-induced currents is 3.01 m/s, the maximum speed, penetration distance and area of rip currents are 1.65 m/s, 124 m and 24 336 m$^2$. The coastal slope not only affects the intensity and range of rip currents, but also has a great influence on their morphological character. The rip currents depicted in Fig. 12b are aggregated as a whole, but are scattered and distributed close to the shoreline in Figs 12d and e. Two additional numerical simulations with coastal slopes of 0.031 and 0.046 were run, in which the rip currents had maximum speeds of 1.99 and 1.77 m/s, penetration distances of 183 and 124 m, and area ranges of 31 011 and 30 153 m$^2$, respectively. The values of wave height increase slowly during the shoreward propagation on the large slope, the surf zones are close to the coastline and their widths are short, thus the rip currents are weak. While on the small slope, the surf zones are far from the coastline, which are not conducive to the longshore current near the coastline, making weak rip currents. Thus, the intensity and range of rip currents first strengthen and then are weakened as the coastal slope increases and the distance of rip current decreases as the coastal slope increases. In all of the five simulations in this paper, the rip currents off a coast-

line with a slope of 0.04 is the strongest.

## 6 Numerical simulations of the influence of coastal size on rip currents

Three coasts of different size were established for rip current simulations. The first is same as depicted in Fig. 7a. The second, shown in Fig. 13a, is half the size of the first, has a flat bottom with water depth of 6.0 m. The third, shown in Fig. 13b, is one-fifth the size of the first, also has a flat bottom with water depth of 2.4 m. In these simulations, the grid space is 1.5×2.0 $m^2$. We uniformly take the incident wave to have a period of 7.0 s and a height of 0.4 m for these simulations. Because the sizes of the three coasts are different, we do not discuss the penetration distance and area ranges of the simulated rip currents, and only present their maximum speeds, 1.49, 1.04 and 0.57 m/s, respectively, corresponding to the first, second, and third coastlines. It seems that the rip currents become smaller as the coastal size decreases.

## 7 Conclusions

In this study, the FUNWAVE model was employed to simulate the rip currents in the Haller experiment and those at an ideal arc-shaped coast similar to the Dadonghai Beach. The results show that the FUNWAVE model is extremely capable to performing the numerical calculations required for the investigation of rip currents. Additional simulations were made to study the rip current characteristics. An arc-shaped coastline was found to be favorable to generate marked rip currents by common waves. These rip currents are greatly influenced by incident waves, and their intensity and range increase as wave height and period increase. The slope of an arc-shaped coast is also shown to have an effect on rip currents; in particular, an overly steep or mild slope is not conducive to the generation of rip currents. With the same incident wave, rip currents were found to become weaker as the size of arc-shaped coast decreased and stronger as its curvature increased.

Since the FUNWAVE model is based on the fully nonlinear

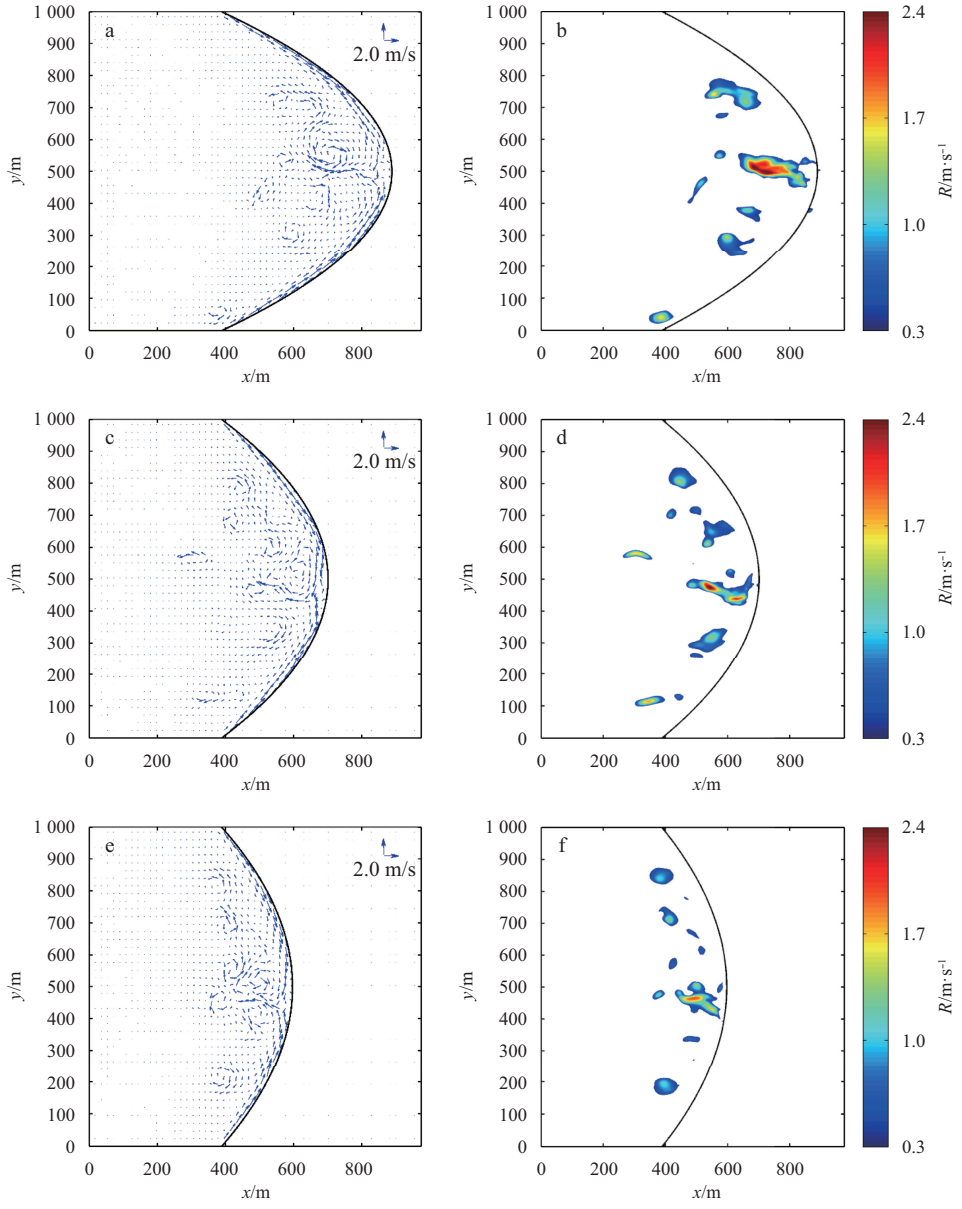


**Fig. 9**

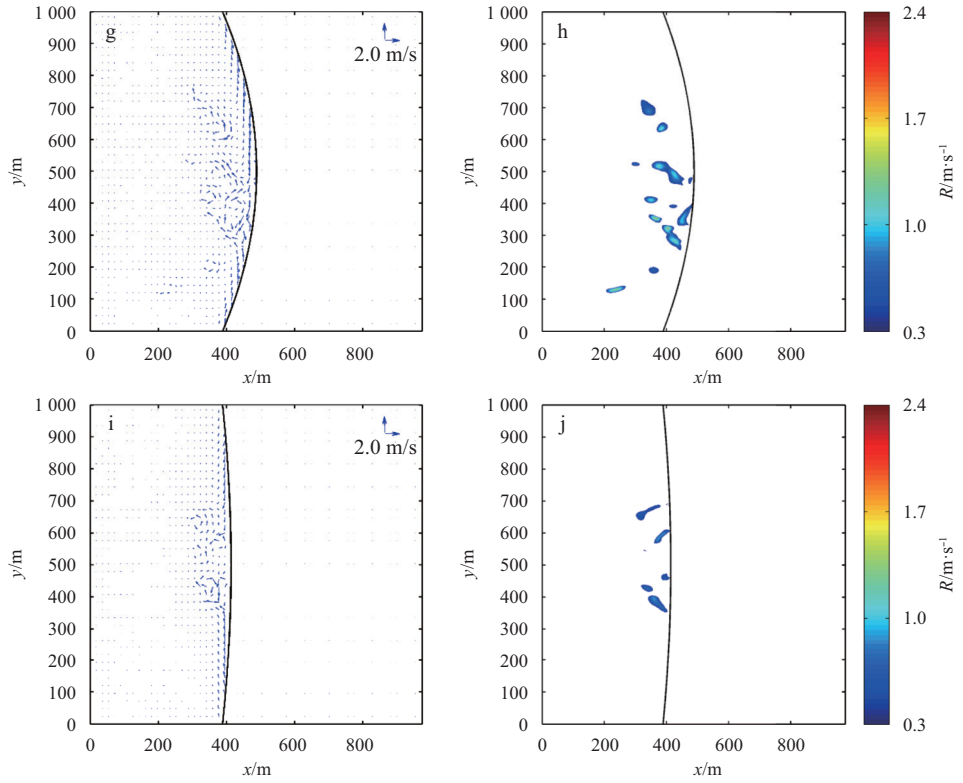


**Fig. 9.** Simulated wave-induced currents and rip currents off arc-shaped coastlines with different curvature (*R* denotes rip current). a. Wave-induced currents for coastline with *k*=0.5; b. range of rip currents for coastline with *k*=0.5; c. wave-induced currents for coastline with *k*=0.3; d. range of rip currents for coastline with *k*=0.3; e. wave-induced currents for coastline with *k*=0.2; f. range of rip currents for coastline with *k*=0.2; g. wave-induced currents for coastline with *k*=0.1; h. range of rip currents for coastline with *k*=0.1; i. wave-induced currents for coastline with *k*=0.03; and j. range of rip currents for coastline with *k*=0.03.

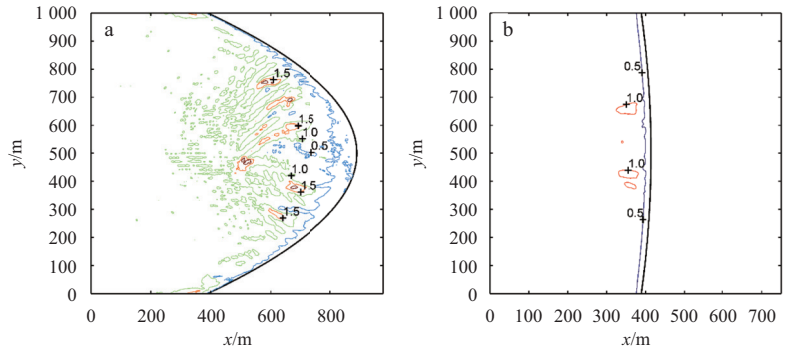


**Fig. 10.** Simulated wave height for coastline with *k*=0.5 (a) and *k*=0.03 (b).

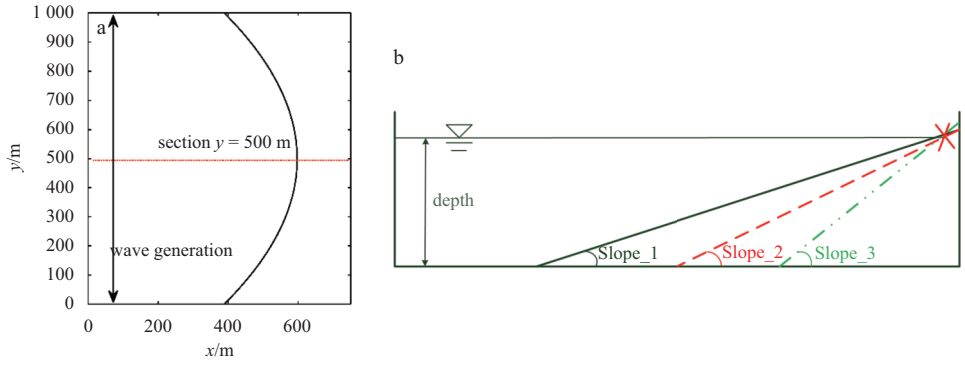


**Fig. 11.** Map of coasts with three different slopes. a. Coastline and section, and b. schematic of water depth in section *y*=500 m.

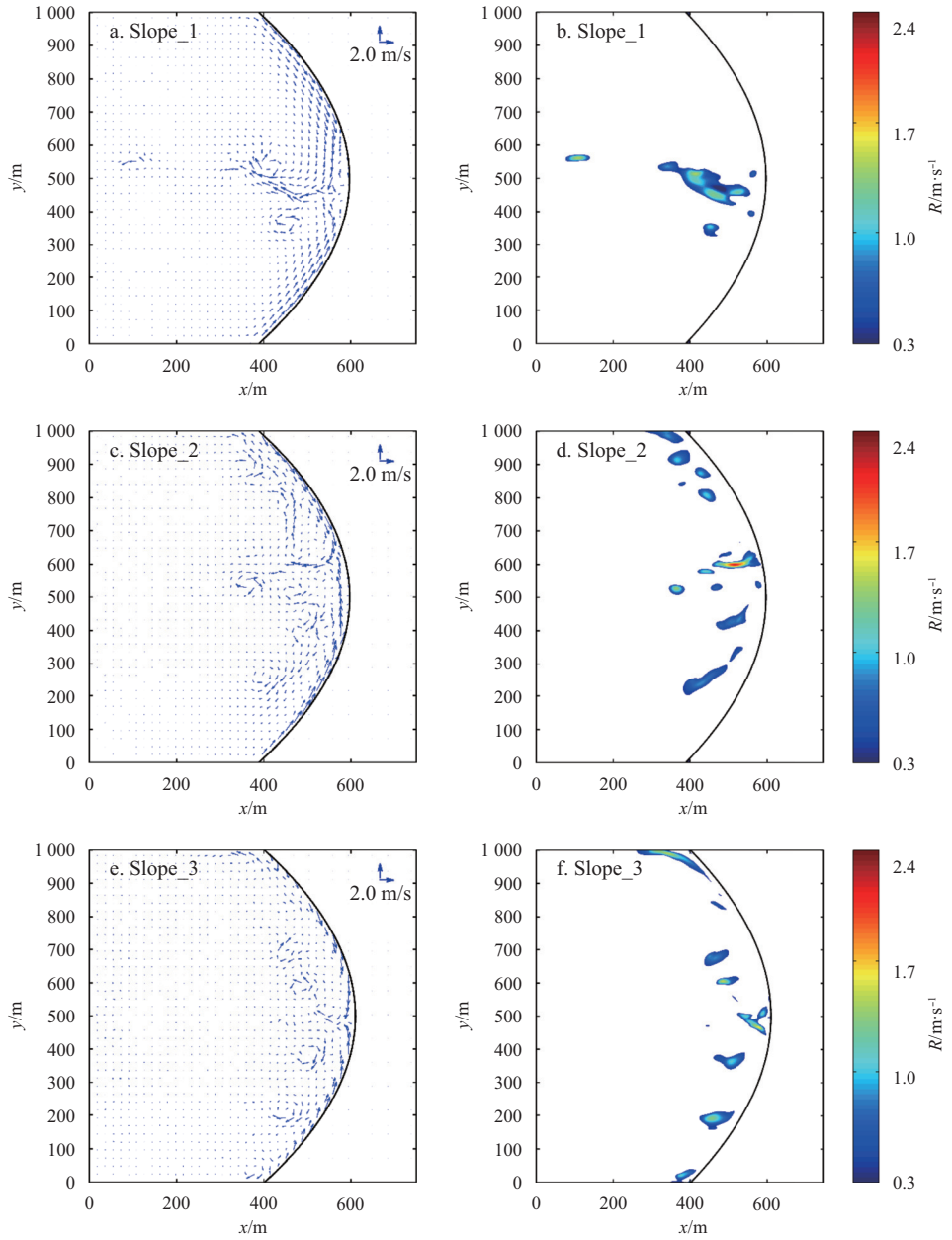


**Fig. 12.** Wave-induced currents (a, c and e) and range of rip currents (b, d and f) for coasts with three different slopes (*R* denotes rip current).

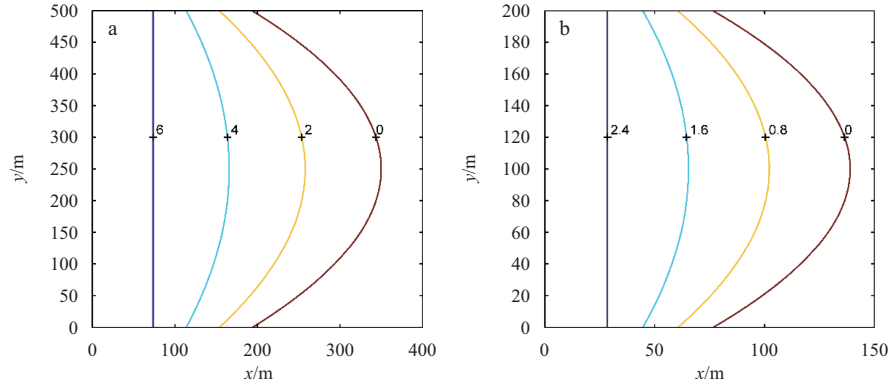


**Fig. 13.** Topography of coasts of different sizes. a. Coast half the size of that depicted in Fig. 7a, and b. coast one-fifth the size of that depicted in Fig. 7a; water depth is in m.

Boussinesq equations, which can reflect the nonlinear characteristics of surface waves and waves breaking near a shore, it can simulate wave-induced flows and rip currents well. However, it takes much computational time because it requires a grid space that is far less than the wave length and a time step much smaller than the wave period. It is not easy to expand the calculation domain to account for the influences of coastal slope and size on rip currents. In future studies, we will use the wave-average model to further investigate the characteristics and dynamic mechanisms of rip currents off arc-shaped coastlines.

**References**

Bae J S, Yoon S B, Choi J. 2013. Boussinesq modelling of a rip current at Heaundae Beach in South Korea. Journal of Coastal Research, 65: 654–659

Bowen A J. 1969. Rip currents: 1. Theoretical investigations. Journal of Geophysical Research, 74(23): 5467–5478

Brown J, MacMahan J H, Reniers A, et al. 2009. Surf zone diffusivity on a Rip-Channeled Beach. Journal of Geophysical Research, 114(C11): doi: 10.1029/2008JC005158

Castelle B, Coco G. 2012. The morphodynamics of rip channels on embayed beaches. Continental Shelf Research, 43: 10–23

Castelle B, Michallet H, Marieu V, et al. 2010. Laboratory experiment on rip current circulations over a moveable bed: drifter measurements. Journal of Geophysical Research, 115(C12): doi: 10.1029/2010JC006343

Chen Qin, Dalrymple R A, Kirby J T, et al. 1999. Boussinesq modeling of a rip current system. Journal of Geophysical Research, 104(C9): 20617–20637

Choi J, Shin C H, Yoon S B. 2013. Numerical study on sea state parameters affecting rip current at Haeundae Beach: wave period, height, direction and tidal elevation. Journal of Korea Water Resources Association, 46(2): 205–218

Dalrymple R A, Macmahan J H, Reniers A J H M, et al. 2011. Rip currents. Annual Review of Fluid Mechanics, 43(1): 551–581

Dean R G, Oh T M. 1994. Three dimensional morphology in a narrow wave tank: measurements and theory. In: 24th International Conference on Coastal Engineering. Kobe, Japan: ASCE, 1918

Drønen N, Karunarathna H, Fredsøe J, et al. 2002. An experimental study of rip channel flow. Coastal Engineering, 45(3-4): 223–238

Fang Kezhao, Zou Zhili, Liu Zhongbo. 2011. Numerical simulation of rip current generated on a barred beach. Chinese Journal of Hydrodynamics (in Chinese), 26(4): 479–486

Giger M, Dracos T, Jirka G H. 1991. Entrainment and mixing in plane turbulent jets in shallow water. Journal of Hydraulic Research, 29(5): 615–642

Ha T, Jun K, Yoo J, et al. 2014. Numerical study of rip current generation mechanism at Haeundae Beach, Korea. Journal of Coastal Research, S72: 179–183

Haas K A, Svendsen I A. 2002. Laboratory measurements of the vertical structure of rip currents. Journal of Geophysical Research, 107(C5): 15-1–15-19

Haller M C, Dalrymple R A, Svendsen I A. 2002. Experimental study of nearshore dynamics on a barred beach with rip channels. Journal of Geophysical Research, 107(C6): 14-1–14-21

Hass K A, Svendsen I A, Haller M C, et al. 2003. Quasi-three-dimensional modeling of rip current systems. Journal of Geophysical Research, 108(C7): 3217

Hsu J R C, Silvester R, Xia Yimin. 1989. Applications of headland control. Journal of Waterway, Port, Coastal, and Ocean Engineering, 115(3): 299–310

Huntley D A, Hendry M D, Haines J, et al. 1988. Waves and rip currents on a Caribbean Pocket beach, Jamaica. Journal of Coastal Research, 4(1): 69–79

Jin Hong, Zou Zhili, Qiu Dahong, et al. 2006. The effects of wave-induced currents on the transport of pollutant outside and inside surf zone. Haiyang Xuebao (in Chinese), 28(6): 144–150

Kennedy A B, Thomas D. 2004. Drifter measurements in a laboratory rip current. Journal of Geophysical Research, 109(C8): C08005

Lascody R L. 1998. East central florida rip current program. National Weather Digest, 22(2): 25–30

Li Zhiqiang, Li Weiquan, Chen Zishen, et al. 2014. Influencing factors and classifications of arc-shaped coasts in South China. Acta Geographica Sinica (in Chinese), 69(5): 595–606

Li Zhiqiang. 2016. Rip current hazards in South China headland beaches. Ocean & Coastal Management, 121: 23–32

Li Zhiqiang, Zhu Yamin. 2015. Beach safety evaluation based on rip current morphodynamic: a case study of Dadonghai of Sanya, China. Tropical Geography (in Chinese), 35(1): 96–102

MacMahan J H, Thornton E B, Reniers A J H M. 2006. Rip current review. Coastal Engineering, 53(2-3): 191–208

Shi Fengyan, Kirby J T, Harris J C, et al. 2012. A high-order adaptive time-stepping TVD solver for Boussinesq modeling of breaking waves and coastal inundation. Ocean Modelling, 43-44: 36–51

Shin C H, Noh K, Yoon S B, et al. 2014. Understanding of rip current generation mechanism at Haeundae Beach of Korea: honeycomb waves. Journal of Coastal Research, 72: 11–15

Short A D. 2007. Australian rip systems-friend or foe? Journal of Coastal Research, S50: 7–11

Wang Yan, Zou Zhili. 2014. Progress and prospect of rip currents. Haiyang Xuebao (in Chinese), 36(5): 170–176

Wei G, Kirby J T, Sinha A. 1999. Generation of waves in Boussinesq models using a source function method. Coastal Engineering, 36: 271–299